This article was published in Surface Science.
Journal homepage: www.elsevier.com/locate/susc
Surface Science 618 (2013) 120–131
DOI: http://dx.doi.org/10.1016/j.susc.2013.09.003

Structure and mass transport characteristics of the surface of gadolinium–doped ceria nanocrystals: Molecular dynamics study.

M.A. Kovalenko[a], A.Ya. Kupryazhkin[a]
[a] Ural Federal University, 620002, Mira street 19, Yekaterinburg, Russia
akm_max@mail.ru kupr@dpt.ustu.ru
Corresponding author: M.A. Kovalenko, akm_max@mail.ru +7(902)8729297,
623704, Berezovsky city, Betonshikov street 9

Abstract

Surface of CGO nanocrystals in a vacuum was investigated by MD method in a wide temperature range with five different potentials. Temperature dependences of distances between cations in near-surface layers in the direction along the surface and to the nanocrystal center were studied in detail. Surface area ratio S(100)/S(111) for equilibrium shape of truncated octahedron has maximum for nanocrystals of 6000-12000 ions.

Surface ion displacement was decomposed on the path along the surface and into the bulk of nanocrystal. The diffusion of surface ions in the entire temperature range has predominantly two-dimensional character, regardless of potentials and the dopant concentration X. Anion diffusion coefficients on the surface and in the bulk were compared, they coincide at T<1200K for X≥0.05. For a system with

X=0.01 anion migration energies of 0.82eV and 0.77eV, and anti-Frenkel pair formation energies of 3.01eV and 4.04eV on the surface and in the bulk, respectively, were obtained.

KEYWORDS: molecular dynamics, cerium dioxide, nanocrystal surface, interatomic distance, surface diffusion.

1. Introduction

Extensive use of materials with submicro- and nanocrystalline structure requires detailed understanding of processes taking place not only in the bulk, but also on the surface and the grain boundary. Cerium oxide (doped with Gd) is a typical representative of such materials and widely used in catalysts, in fuel cells and as a structural analogue of oxide nuclear fuel. At the same time, processes occur on the surface of the crystal often can serve as some equivalent of processes in grain boundaries, and essentially differ from similar processes in the bulk of the crystal.

Experimental studies of the crystal surface are focused in general to the definition of the structure and defect formation energies on the surface, especially on reduced surfaces, and on surface exchange reactions [1–5]. Serious difficulties in experimental researches are the imperfection of the surface, impurities in the sample (which are often even at threshold valuations of concentration can significantly affect surface properties), as well as different processes concurrently occur on the surface, which can't always be separated. Mass transport processes on the surface are still poorly experimentally explored. Investigation of sintering processes, including nano-powders, is one of the most important technological objectives. However, for a complete understanding of these processes mass transport processes on the ideal nanocrystal surface at different temperatures should be thoroughly examine.

Computer simulation methods can perform experiments with fully-controlled conditions. Despite the development and successes of quantum-chemical methods, at present time they can determine, in general, only static characteristics of the surface, such as the electronic structure of surface ions, or the formation energy of surface defects. A good overview of calculation results of the above parameters and their comparison with experiment results, as well as comparison between different quantum-chemical methods, can be found in [6]. Quantum-chemical methods in the present time do not allow obtaining diffusion coefficients over a wide temperature range, which define the characteristics of ceramic materials having high surface area. Therefore, the molecular dynamics (MD) method, with all its limitations, is still the most attractive for simulations of mass transport characteristics on the surface of nanocrystals.

Main limitations of the MD are invariable pair interaction potentials and neglect of the electron density redistribution near defects and on the surface. However, for ionic systems the question of the adequacy of pair potentials using is not as critical as, for example, for metals. So, the classical MD method with pair potentials reproduces superionic transition (melting of the anion sublattice, while the cation sublattice stays in the crystalline state) at which the defect concentration exceeds 30% of the anion number. It was shown in [7] that superionic transition takes place for all investigated potentials during simulations under periodic boundary conditions, but for finite nanocrystals in vacuum with most of potentials melting occurs before superionic transition.

The aim of this work was to investigate the disorder and defect formation in near-surface layers, and especially the self-diffusion of surface ions, in $Ce_{1-X}Gd_XO_{2-X/2}$ nanocrystals with various dopant concentrations X, in a wide range of temperatures from room to melting temperature. To determine the influence of a specific pair potential set on simulation results four different potentials, obtained by fitting to the experimental data and to the results of quantum-chemical calculations, have been investigated.

2. Simulation method

2.1. MD details

In this paper we used the classical MD method, with pair interaction potentials in the rigid ion approximation, which is justified for ionic crystals and saves computational resources. We investigated finite nanocrystals in vacuum - the so-called zero boundary conditions. MD realization, one of the used in the present study pair potential set (PPS) KMKA12 and the calculation of nanocrystal volume characteristics were described in detail in [8]. The most resource-intensive part of the simulation – calculation of long–range Coulomb forces – was carried out on graphics processors Ati Radeon 6970, which significantly increased the duration of the MD simulation in comparison with the classical realization on the CPU.

We investigated nanocrystals using different PPS (in the brackets the year of development is indicated): KMKA12 (2012) [8], Inaba (1999) [9], Gotte2007 (2007) [10], Grimes (1999) [11] and Cui (2011) [12]. Although the Gotte2007 and Grimes PPS were derived in the shell-model approximation, we used it in rigid ion approximation, like some others [13]. Shell-model approximation not only requires 4 times more in the computational cost for MD step, and a substantially smaller time step, but it gives underestimated values of the anion migration energy compared with the rigid ion approximation. For all PPS except Gotte2007 we used the MD step equals to 3.5 fs.

Cui potentials were derived from *ab initio* quantum-chemical calculations in the rigid ion approximation with formal ion charges, and other PPS are semi-empirical.

2.2. Equilibrium shape of nanocrystals

The fluorite crystal lattice of cerium dioxide and CGO solid solutions is cubic. Initial nanocrystals were created in a cubic form with a (100) surface type, and to eliminate the surface charge we used such unit cell that gives only the half

of oxygen ions on the outermost surface layer compared with the number in the bulk crystal plane. Actually, it was demonstrated in experiments [14] that the crystal surface (100) is arranged in this manner. Nevertheless, the most energetically favorable surface type for fluorite crystal lattice is (111) surface. Initial cubic nanocrystal was simulated by MD in an ordinary way at a temperature a little lower than melting temperature, and it shape transformed by ions mass transport, without any additional influence. Truncated octahedral shape of nanocrystal was also obtained in [15] by amorphisation and recrystallisation of the initial cubic nanocrystal. Nanocrystal was artificially expanded by about 35%, but octahedral shape was achieved by considerably lower simulation times.

Previously in [8] the relaxation of pure CeO_2 nanocrystal with cubic shape to its equilibrium state with a shape of truncated octahedron (also called the Wulff shape) was shown with KMKA12 potential. Nanocrystals of solid solution with Gd dopant relax in the same manner, as shown in Fig.1 for KMKA12 and Inaba PPS.

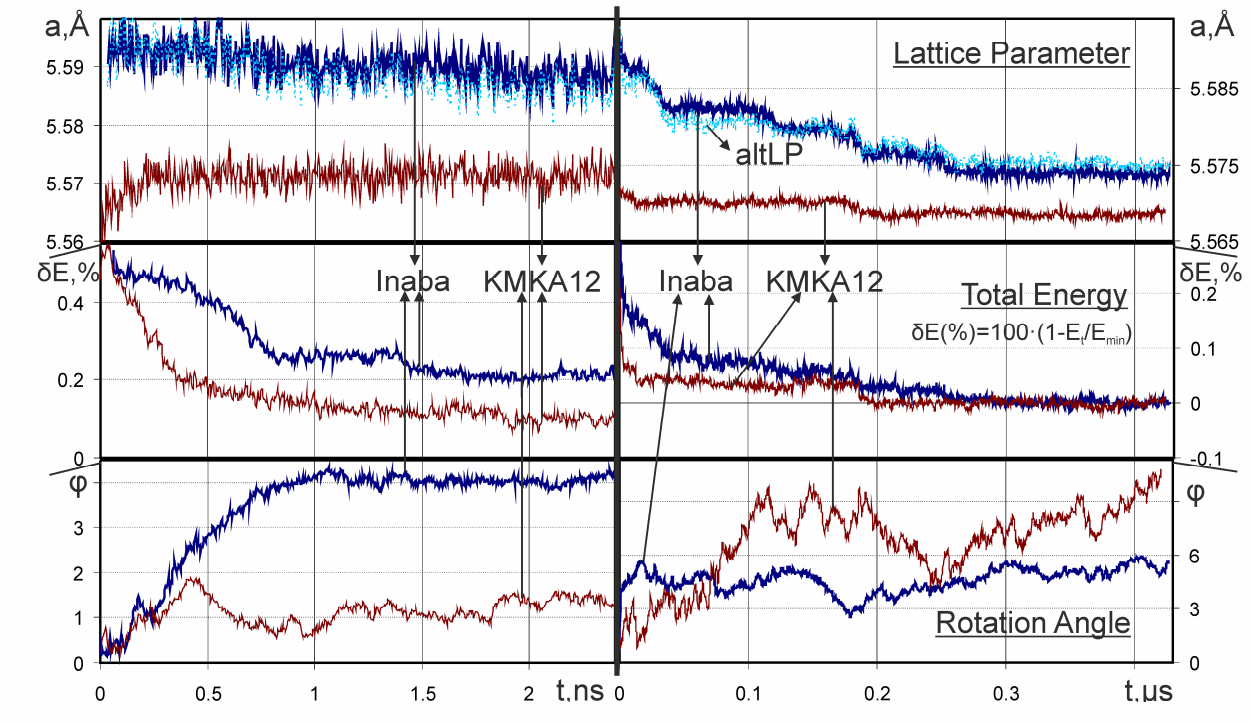

Figure 1. Lattice parameter and total energy evolution of $Ce_{0.8}Gd_{0.2}O_{1.9}$ nanocrystals, as well as the rotation angle of the (100) crystallographic plane. The number of particles was 5939, simulation temperature was 2000K for KMKA12 PPS and 2500K for Inaba PPS, and in both cases was approximately equal to 0.8 of melting temperature. Simulations were carried out

during about 120,000,000 MD steps. "AltLP" means the lattice parameter derived from the distances between the cation crystal planes in the inner region of nanocrystal.

It follows from the data in Fig. 1 that the relaxation process is finished at about 0.25 μs (70,000,000 MD steps), but visually nanocrystals take octahedral shape much earlier, at about 10 ns (3,000,000 MD steps). “Alternative” lattice parameter “AltLP”, derived from distances between cation crystal planes in the inner region of the nanocrystal, is shown in Fig. 1 for Inaba PPS. Since this method is insensitive to vacancies in the cation sublattice (in contrast to calculation from numerical density of cations), the coincidence of lattice parameter curves means that cation vacancies were not generated in the bulk by any reason. Octahedral surface compresses the inner region of the nanocrystal more strongly than cubic surface, which results in decreasing of the lattice parameter.

An important issue is the rotation of the nanocrystal, which can take place as a result of calculation errors or absence of the correction of the moment of rotation. Since diffusion coefficients are derived from the mean square displacement (MSD) of ions, the rotation may introduce significant errors to calculated values. It follows from the data in Fig. 1 that the rotation of the nanocrystal can be ignored after the relaxation to the octahedral shape, and some random precession of the crystal plane vector is determined by random local mass transport of ions on the surface. The initial rotation (first 0.1 ms) is caused by, apparently, uneven redistribution of ions from corners of the initial cubic nanocrystal to corners of the relaxed octahedron.

2.3. Separation of the nanocrystal surface

The surface should be determined dynamically during the simulation, because nanocrystal can rotate and its form can change. Therefore, we can’t determine the surface at the beginning of the simulation and avoid uncontrolled errors - as it will be shown below the motion of ions at the surface and in the bulk is essentially different.

Our procedure is based on the selection of the cation surface layer, as in fluorite systems their mobility is much smaller than anion mobility. Surface cations and anions in the XY 2D-plane, and the general 3D-view of the nanocrystal with the shape of truncated octahedron, are shown in Fig. 2.

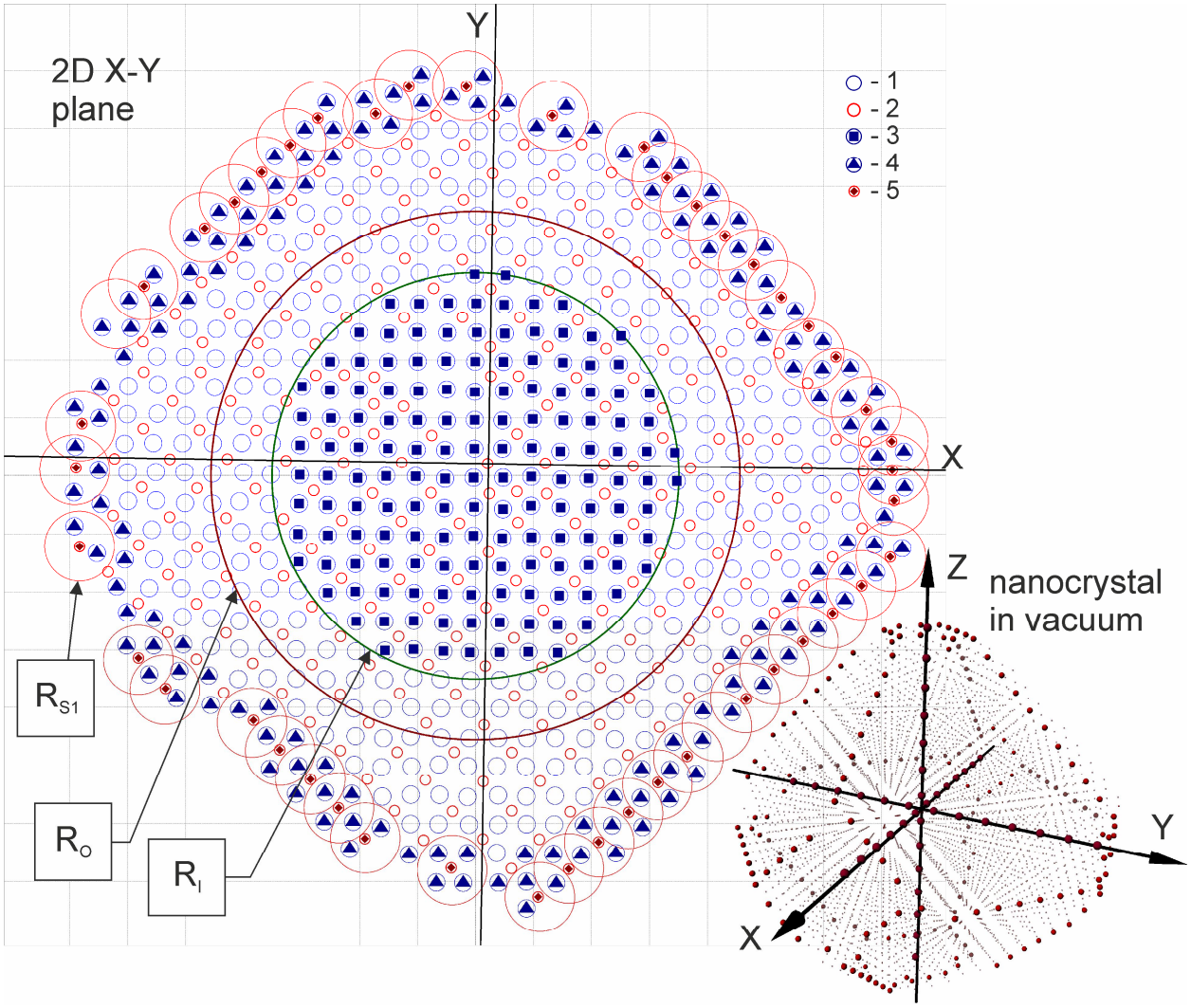

Fig.2. Selected surface and volume regions of the nanocrystal in the 2D-projection. 1 – anions, 2 – cations, 3 – volume anions (which participate in the volume MSD calculation), 4 and 5 – surface anions and cations respectively, and surface MSD are calculated by their positions. Right bottom insert shows a 3D-view of relaxed nanocrystal in a vacuum with octahedral shape.

Every N MD steps (100 in this work) by the averaged during these steps cation coordinates we determined cations with the number of nearest neighbors less than 12 (and 12 is the number of nearest cations in a perfect fluorite lattice). At the position of each of these cations we created the so-called surface center, with the radius R_{S1} equals to 0.6 of lattice parameter. All of these detected surface centers (spheres with R_{S1}) will be the surface of the nanocrystal, which certainly can

change during simulation. As a surface anion we considered anion that falls into any of surface centers, and anion surface layer in this study formally consists of the outmost and the next to the surface anion crystalline planes.

To speed up calculations the chained cells were extensively used, see for example [16].

2.4. Calculation of (111) and (100) nanocrystal surface areas and near-surface interatomic distances

Nanocrystal in its equilibrium shape during the simulation has only surfaces of the (111) and (100) type, so we will investigate only them and other types of surfaces will not be artificially created.

Let's assume that the simulated nanocrystal has its equilibrium shape of a truncated octahedron and we already detected the surface as a set of surface centers. Knowing vectors of cation crystalline planes (they do not coincide with global space vectors due to the rotation of nanocrystal) we compute vectors and approximate positions that define (100) and (111) planes of truncated octahedron surfaces. Then we refine the position of each plane by averaging coordinates of surface cations that are close to it. Plane vectors remain unchanged. The intersection of planes found will give coordinates of vertexes of polygons (facets) which approximate the nanocrystal surface. As a result, we get vertex coordinates of six rectangles, corresponding to the (100) surface, and eight hexagons, corresponding to the (111) surface, as shown in Figure 3.

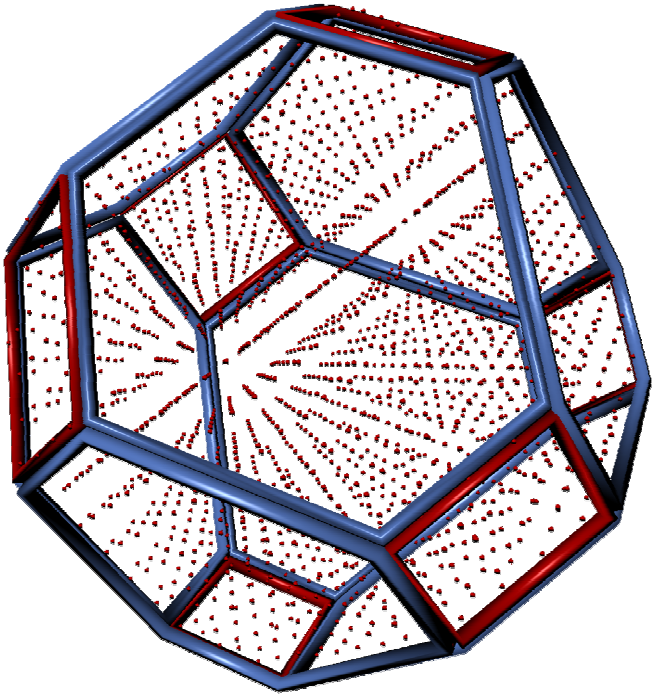

Fig. 3. An example of the nanocrystal surface approximated with polygons. Only the cation sublattice of the nanocrystal consisted of 6144 ions is shown. Red rectangles approximate the (100) surface and blue hexagons – the (111) surface.

This procedure was carried out every 500 MD steps. Knowing the vertex coordinates one can determine facet areas and the (100) to (111) area ratio, which, in turn, determines the corresponding surface energy ratio.

For each hexagonal facet we determined cations lying in the first, second and next near-surface layers. We analyzed five near-surface layers and accordingly received four interatomic distances (IAD) between the nearest cations in the adjacent surface layers. The above distances show contraction or expansion in the perpendicular direction to the (111) facet (or to the nanocrystal center). It is interest to determine interatomic distances between nearest cations belong to a given (111) plane for each of five subsurface layers (in the tangent direction to the surface). For (100) surface we determined only surface and next to surface layers, and similarly calculated normal IAD between layers and tangent IAD inside the outmost surface layer.

The calculation of near-surface IAD was performed by successive heating or cooling of the nanocrystal with temperature increment of 50–100 K during 0.175 ns (50,000 MD steps) for a given temperature. In order to confirm adequacy of this

duration we simulated nanocrystal of 6144 ions under same conditions, but averaged IAD were calculated during 2.1 ns (600,000 MD steps) at a given temperature. Largest deviations of the order of 0.001Å (0.025% of the lattice parameter) were observed for the IAD on truncated corner of the octahedron with (100) surface type, due to the relative small number of cations on these facets. For other IAD relating to (111) facets deviations were 0.0001Å and less.

2.5. Calculation of surface diffusion coefficients and displacement of surface ions along the surface and into the volume of nanocrystal

According to the random walk theory the diffusion coefficient can be determined by the mean square displacement (MSD) of ions:

$$\lim_{t\to\infty}\left[\frac{1}{N}\sum_{I}(\mathbf{r}_I(t)-\mathbf{r}_I(0))^2\right]=C\cdot D\cdot t \qquad (1)$$

where t is the simulation time, N the number of ions for MSD calculation, $\mathbf{r}_I$ the position of the "I" ion, D is the diffusion coefficient. Constant C equals to 6 in the 3D-case and to 4 in 2D-case.

To determine diffusion coefficients in the nanocrystal of finite size we should separate volume and surface regions. To calculate MSD in the volume region of the nanocrystal at some moment t_R we saved indexes and coordinates of "inner" ions falling into the sphere of radius R_I (Fig. 2). During the simulation we saved ion coordinates $\mathbf{r}_I(t)$ and found a number of ions which went out of the sphere with radius $R_O>R_I$. When this number exceeded 30% of the original number of "inner" ions, we detected ions that came to the surface at least once during the simulation and exclude them from MSD calculation. Then we again detected "inner" ions in the inner region and so on, and the final MSD graph had a sawtooth nature.

MSD calculation of surface ions of the given type was carried out in a similar way. At some moment t_R we detected indexes and saved coordinates of those ions whose distance to at least one of surface centers was less than R_{S1} equals

to 0.6 of the lattice parameter (distance between the first and second anion neighborhood for the cation, see Fig. 2). Thus we chose the outermost surface and next to the surface anion planes. During the simulation we saved coordinates of selected surface ions, checked ions that should be excluded by some conditions, and when the number of these "excluded" ions exceeded 30% of surface ions we calculated MSD by all surface ions.

In contrast to volume MSD for surface MSD we assigned two conditions for detection of "excluded" ions. The first condition fulfils when the ion has moved a distance greater than 1.6 of the lattice parameter for each of surface centers. This condition corresponds to the situation when ion has moved from the surface to the volume of nanocrystal. The second condition fulfils when the distance from the current ion position to its initial position at the moment t_R exceeds half of the octahedron diagonal. This condition ensures that the ion will not travel on the front surface and return to its original position on the back surface of the nanocrystal. Without these conditions surface MSD will go out on the plateau similar to volume MSD, as was shown in [8]. Surface MSD graph also had a sawtooth nature.

Surface ions can move along the surface and into the bulk of the nanocrystal. Let’s decompose the ion displacement vector (the difference between positions at the current moment and at the initial moment t_R) on tangent and normal components. For that we approximate the nanocrystal surface by an equivalent sphere, because the nanocrystal shape of the octahedron with truncated corners is relatively symmetric. Method of calculation of the path that ion moved along the surface (tangent) and to the center of the sphere (normal), for simplicity reduced for two-dimensional case, is shown in Fig. 4 on the left side.

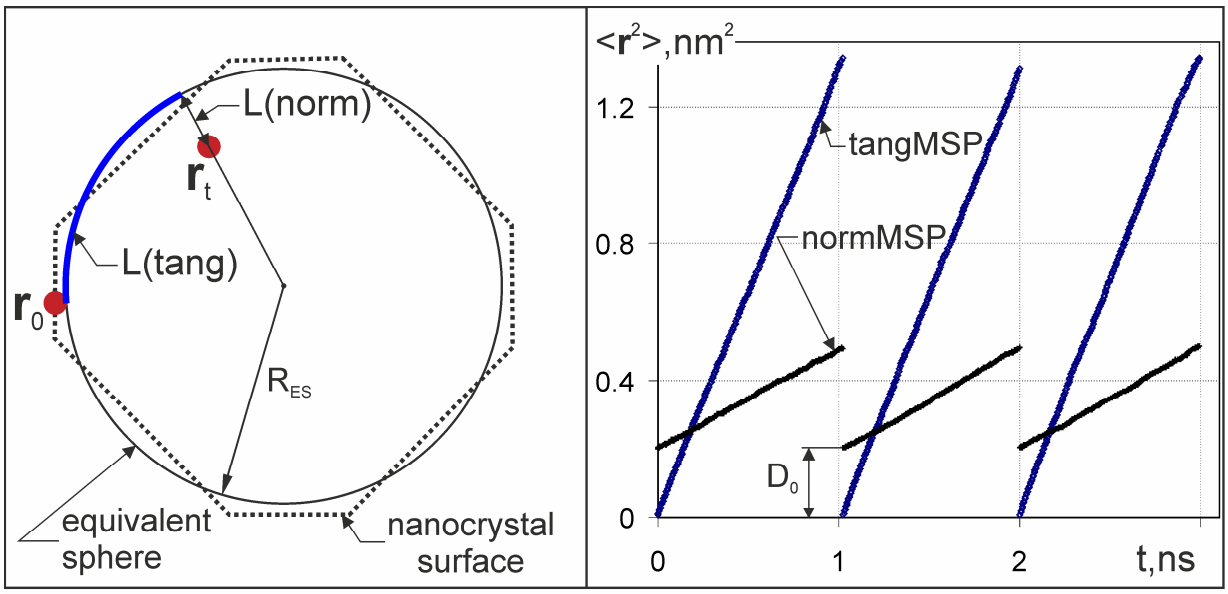

Fig. 4. On the left side the scheme of the surface ion path decomposition on the tangent and normal components is shown. $\mathbf{r}_0$ and $\mathbf{r}_t$ are ion positions at initial and the current moment t, L (norm|tang) is the path moved by the ion assuming that nanocrystal shape is some equivalent sphere. On the right side the result of separate calculation of mean square path (MSP) of ions in tangent and normal directions is shown. Simulated system consisted of 39,150 ions (X = 0.2) with KMKA12 potential at T=1450 K.

The center of mass of the nanocrystal is at the origin in global space. The equivalent sphere radius R_{ES} we calculated as the average length of position vectors of surface cations (both Ce and Gd cations in the case of ternary system). The path which ion moved at the moment t along the surface and into the volume of equivalent sphere is defined as:

$$\begin{aligned} L(\text{tang}) &= R_{ES} \cdot \arccos(\mathbf{r}_0 \cdot \mathbf{r}_t / (|\mathbf{r}_0| \cdot |\mathbf{r}_t|)) \\ L(\text{norm}) &= R_{ES} - |\mathbf{r}_t| \end{aligned} \qquad (2)$$

where $\mathbf{r}$ is the position vector of the ion at t=0 or at the current moment t. Similar with the MSD definition we can define the mean square path (MSP) walked by surface ions along the surface of the equivalent sphere and perpendicular to it:

$$\text{tangMSP} = \sum_{I=1}^{N} L_I^2(\text{tang}) / N, \quad \text{normMSP} = \sum_{I=1}^{N} L_I^2(\text{norm}) / N \qquad (3)$$

where N is the number of surface ions of the given type. The value of D_0 in Fig. 4 determines the deviation of octahedron shape from ideal sphere at the initial moment.

It can be seen from Fig. 4 that mean square tangent and normal paths of ions are well described by a straight line, though we have no reasons to associate these angles of slope with diffusion coefficients. Let's define the value of the displacement along surface coefficient (DaSC) as the ratio of angles of slope of tangMSP to normMSP curve. This DaSC value will numerically characterize the fraction of the ion movement along the surface, and based on it we can conclude whether ions move mainly along the surface or into the nanocrystal volume.

3. MD simulation results and discussion

3.1. Surface relaxation and equilibrium surface structure

Approximation of the nanocrystal surface shape by the sphere can characterize the process of nanocrystal shape evolution during the simulation. Results of this approximation for CeO_2 system of 6144 ions with KMKA12 potential are shown in Fig. 5.

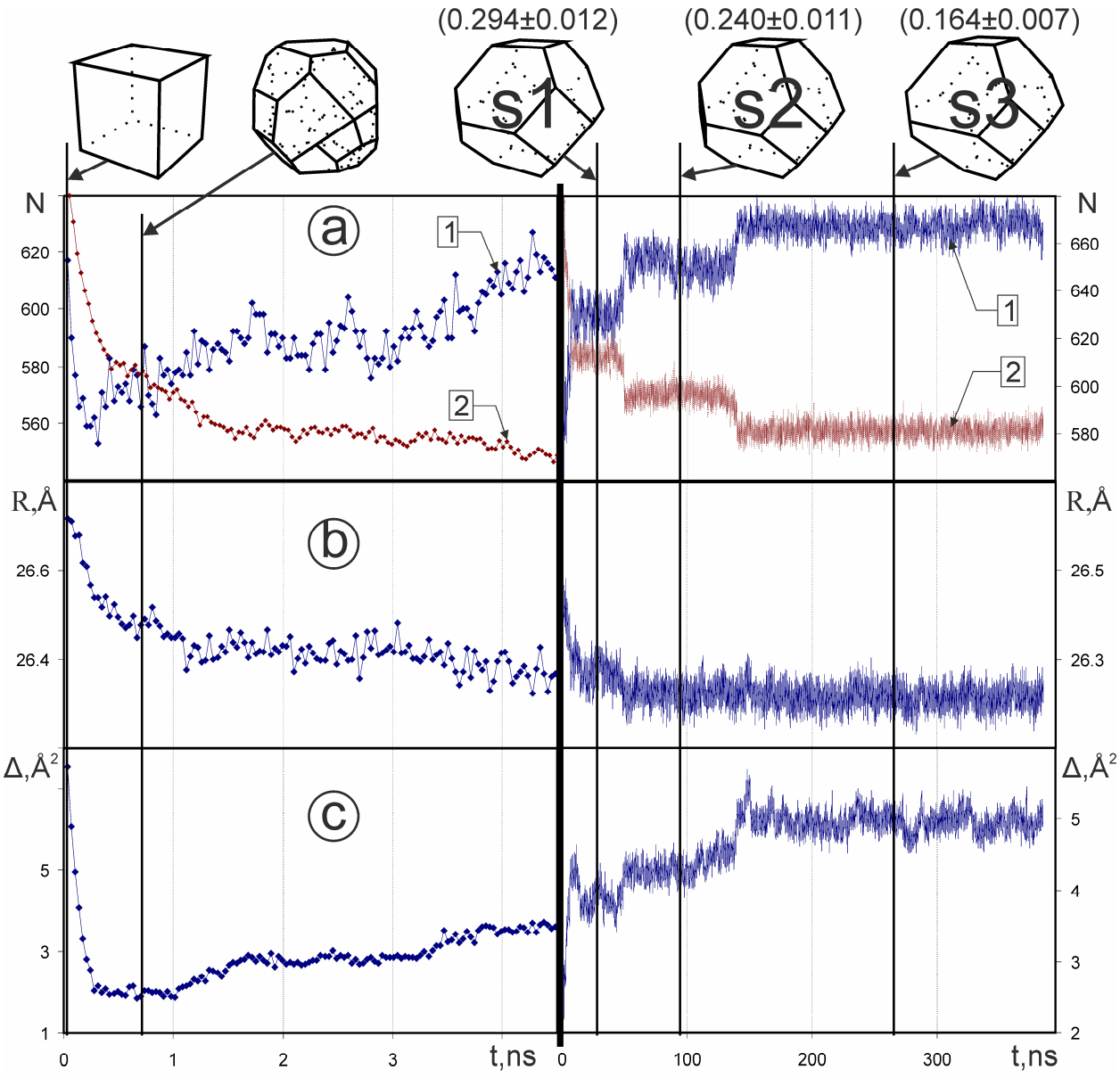

Fig. 5. Equivalent sphere approximation of the surface of CeO_2 nanocrystal consisted of 6144 ions with KMKA12 potential during the simulation at T=2200 K. On the left side the initial period of relaxation and on the right side the entire simulation period are shown. (a) - the number of detected surface centers (1) and the nanocrystal total energy (2), (b) - the radius of the equivalent sphere, (c) - mean square displacement of ions from equivalent sphere surface. The above figures show the nanocrystal shape at the simulation time indicated by the corresponding vertical line, and numbers show the ratio of (100) to (111) surface areas of truncated octahedron at a given time.

It follows from the data in Fig. 5 that for the given temperature initially created cubic nanocrystal deforms during first 100,000 MD steps, and minimums on graphs (a-1) and (c) on the left side correspond to the surface shape closest to the sphere. Step change on the total energy curve (a-2) on the right is correlated

perfectly with the surface center number (a-1). It is interesting to investigate nanocrystal shapes before and after these step transitions, and the comparison of nanocrystal shapes approximated by truncated octahedron is shown in Fig. 6.

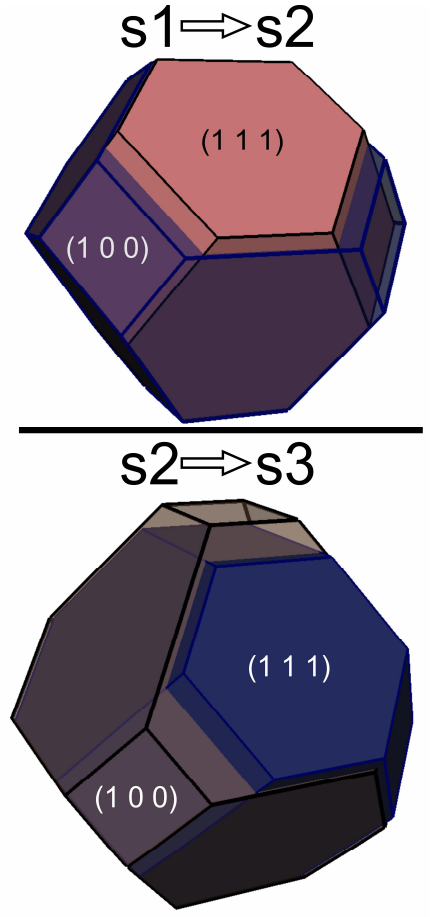

Fig. 6. Evolution of the nanocrystal with the shape of truncated octahedron. Shapes s1, s2 and s3 correspond to shapes on the top of Fig. 5. Solid truncated octahedron corresponds to the crystal before transition and transparent – after transition.

In both cases the mechanism of shape changing is the same and consists in the migration of surface cations from one (111) facet to two adjacent (100) facets. This increases the (111) surface area and decreases the (100) surface area, as well as increases the number of surface centers.

Initially created cubic nanocrystal had the (100) surface with only the half of oxygen ions in the outmost crystal plane. When the nanocrystal relaxed to the shape of truncated octahedron the (111) facet became uncharged and the outmost crystal plane was completely filled with oxygen ions, same as (111) oxygen terminated surface created in quantum-chemical calculations. The (100) facet of truncated octahedron had a half-filled oxygen outmost crystal plane same as the

original cubic crystal surface. Visually we observed that (111) facets were almost always perfect and filled, on truncated corners (100) of octahedron prominent ions (single or in a form of a step) were frequently observed, and sometimes cations at the intersection of two (111) facets near the truncated corner were missed. A more detailed study of surface defect types and their numerical calculation is beyond the scope of this paper.

In [17] authors investigated surface structure from thermodynamic point of view and concluded that for the (111) surface the oxygen terminated surface type is the most advantageous, and for (100) surface the outermost layer should consist of cerium ions. But they did not consider the version with half-filled oxygen outmost layer on the (100) surface, and in general their conclusions coincide with results of our calculations.

3.2. Areas of (111) and (100) facets of nanocrystals with truncated octahedron shape

Nanocrystal shape evolution obviously associated with the cation diffusion process and has the comparable characteristic time and the exponential temperature dependence. Although cation diffusion on the surface is much faster than in the bulk, the existing computing power didn't allow us to directly calculate temperature dependences of equilibrium ratio of (100) to (111) facet areas of the truncated octahedron S(100)/S(111), especially for large systems . However for a small system of 1500 ions prolonged simulation revealed no difference between S(100)/S(111) ratios at temperatures of 1950 K and 1500 K. Area ratios of $Ce_{1-X}Gd_XO_{2-X/2}$ nanocrystals of different sizes for a given relatively high temperature are summarized in Table 1. Simulations were carried out during about 0.5 μs.

L, nm	N	Potentials set	T, K	T/T_m	S(100)/S(111)
X=0					
4.5	1500	KMKA12	1950	0.81	0.090±0.012
5.6	2592	KMKA12	2100	0.83	0.148±0.009

7.7	6144	KMKA12	2200	0.82	0.164±0.007
9.7	12000	KMKA12	2300	0.84	0.175±0.007
9.7	12000	Cui	3700	0.85	0.177±0.006
14.9	40500	KMKA12	2500	0.91	0.152±0.006
X=0.2					
4.5	1450	KMKA12	1650	0.79	0.082±0.016
5.6	2506	KMKA12	1900	0.84	0.127±0.014
7.8	5939	Inaba	2500	0.8	0.171±0.012
7.7	5939	KMKA12	2000	0.83	0.217±0.014
9.8	11600	KMKA12	2300	0.91	0.211±0.009
14.9	39150	KMKA12	2350	0.93	0.141±0.004
Experiment					
4-6	[17]	---	300	0.12	0.03±0.01
200-500	[18]	---	300	0.12	0.0616±0.0194

Table 1. Surface area ratios of (100) to (111) facets of nanocrystals with the shape of truncated octahedron. Values of L denote the characteristic size (diagonal) of truncated octahedron, and values of T/T_m show the ratio of the simulation temperature to the melting temperature of the nanocrystal of a given size.

Results of our simulations show that for the nanocrystal size of 8-10 nm (6,000-12,000 ions) surface area ratios S(100)/S(111) had a maximum. At that these ratios are greater for nanocrystals with Gd dopant than for pure CeO_2 nanocrystals. Selective simulations of nanocrystals with Cui and Inaba PPS showed that interaction potentials influence not very strong on the resulting S(100)/S(111) ratio.

It should be noted that for small crystals (100) facets are often not completely filled during simulation and steps with prominent ions are observed. Our procedure for octahedron truncated corner approximation handles all surface centers, which leads to a certain shift of the (100) facet toward the nanocrystal center and thus to an increase of S(100)/S(111) ratio. In experimental studies during two-dimensional images processing the presence of cation steps leads on

the contrary to a decrease of S(100)/S(111) ratio, which should be take into consideration when comparing with simulation results.

3.3. Temperature dependences of cation interatomic distances in near-surface layers of nanocrystals with the shape of truncated octahedron

Anions in fluorite systems are very mobile, and for KMKA12 potential even superionic transition in nanocrystals at high temperatures (the melting of the oxygen sublattice) is observed – so interatomic distances (IAD) for surface and near-surface anions in this study were not calculated, and only the cation sublattice was processed.

As already mentioned in section 2.4 for the investigation of cation locations in (near-)surface layers we defined four IAD types between them – in the normal and tangent directions for (111) facets and the same for (100) facets. Comparison of IAD temperature dependences for nanocrystals of different sizes of 6144, 12000 and 40500 ions with KMKA12 potential showed that IAD are almost independent from the size of the simulated crystal. Therefore further comparisons with different PPS would be carried out with nanocrystals of 12,000 ions for dopant concentration X=0.0 and with nanocrystals of 11,600 ions for X=0.2. The lattice parameter in the nanocrystal volume for comparison with surface IAD was converted into IAD by dividing it by $\sqrt{2}$. Temperature dependences of normal (between the cation belongs to the first and nearest cations belong to the second surface layers) and tangent (between adjacent cations belong to the outmost surface layer) distances for faces (111) and for truncated corners (100) with four PPS are shown in Fig. 7.

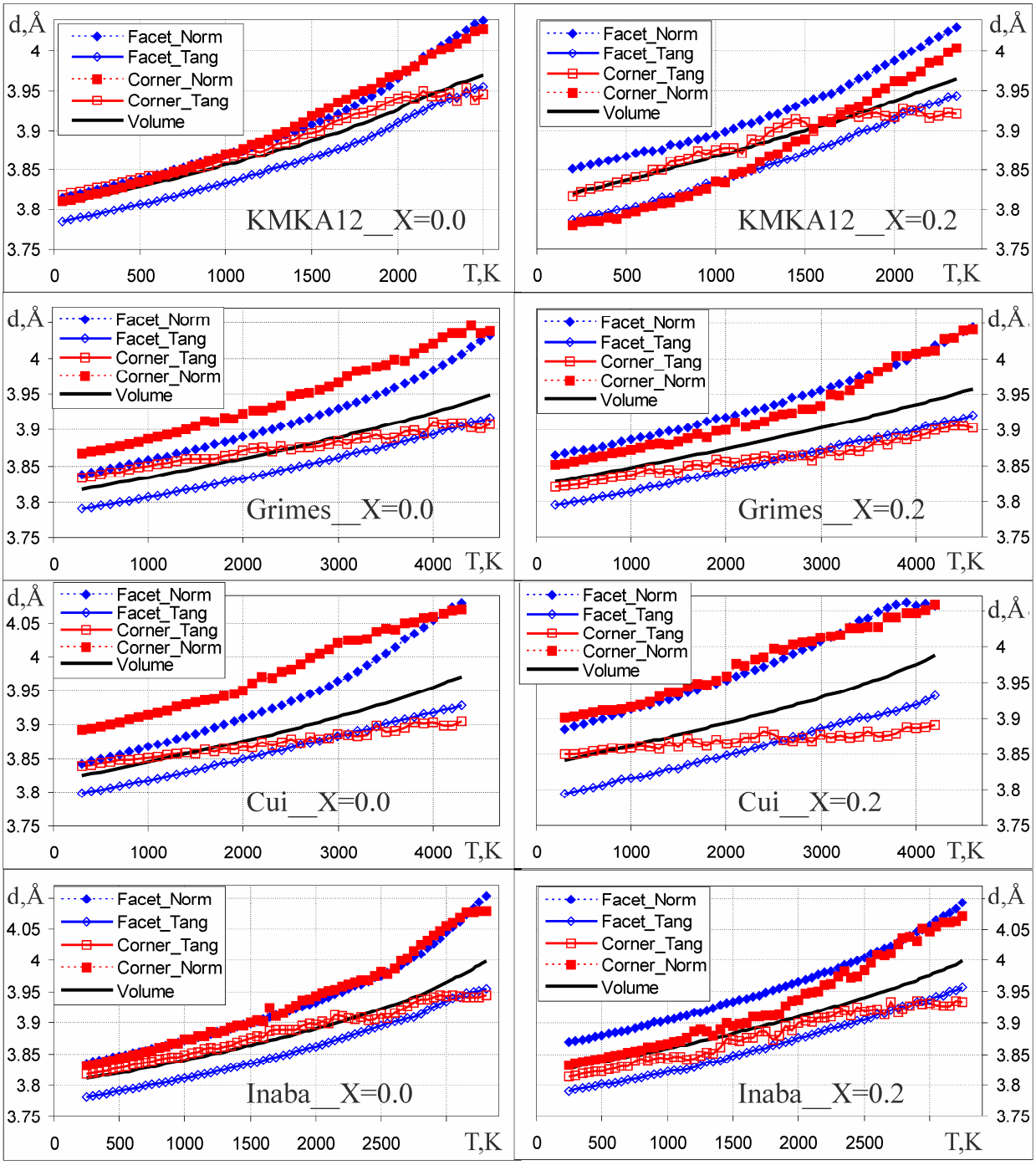

Fig. 7. Temperature dependences of interatomic distances, "Facet_" means IAD for the (111) surface type and "Corner_" for the (100) surface type. Comparisons were carried out with four potential sets for CeO_2 systems with X=0.0 and $Ce_{0.8}Gd_{0.2}O_{1.9}$ with X=0.2. If the IAD value in the normal or tangent direction exceeds the volume value than the surface is expanded in this direction, and vice versa.

From the data in Fig. 7 one can see the following common features that are typical for all PPS studied:

1) For (111) facets cationic planes are expanded (in the normal direction to facets) in comparison with the nanocrystal volume, but cations inside the outmost (111) facet are contracted (in the tangent direction). These effects are more pronounced for systems with impurity.

2) As the temperature increases the distance between cationic planes on the surface grows faster than in the volume of the nanocrystal.

3) In all cases tangent distances on (100) facets at a certain temperature stop the increasing, and graphs become almost horizontal.

Let's compare in detail deviations of surface IAD from the bulk one with different potentials. For a given temperature the deviation of a surface distance from the volume (in percentage) we defined as:

$$\delta_X = 100 \cdot \left(1 - \sqrt{2} \cdot X/a\right) \quad (4)$$

where X is the averaged distance between nearest cations (tangent for cations belong to a given plane, normal distance for cations belong to different adjacent planes), a is the bulk lattice parameter. The positive δ_X value means expansion of cationic planes and the negative value means contraction. For nanocrystal (111) facets we defined five (near-)surface cationic planes and, respectively, studied four interplanar distances and five tangent IAD characterizing expansion-contraction of the facet parallel to the (111) surface. Temperature dependences of normal IAD deviations for (111) facets for all PPS are shown in Figure 8.

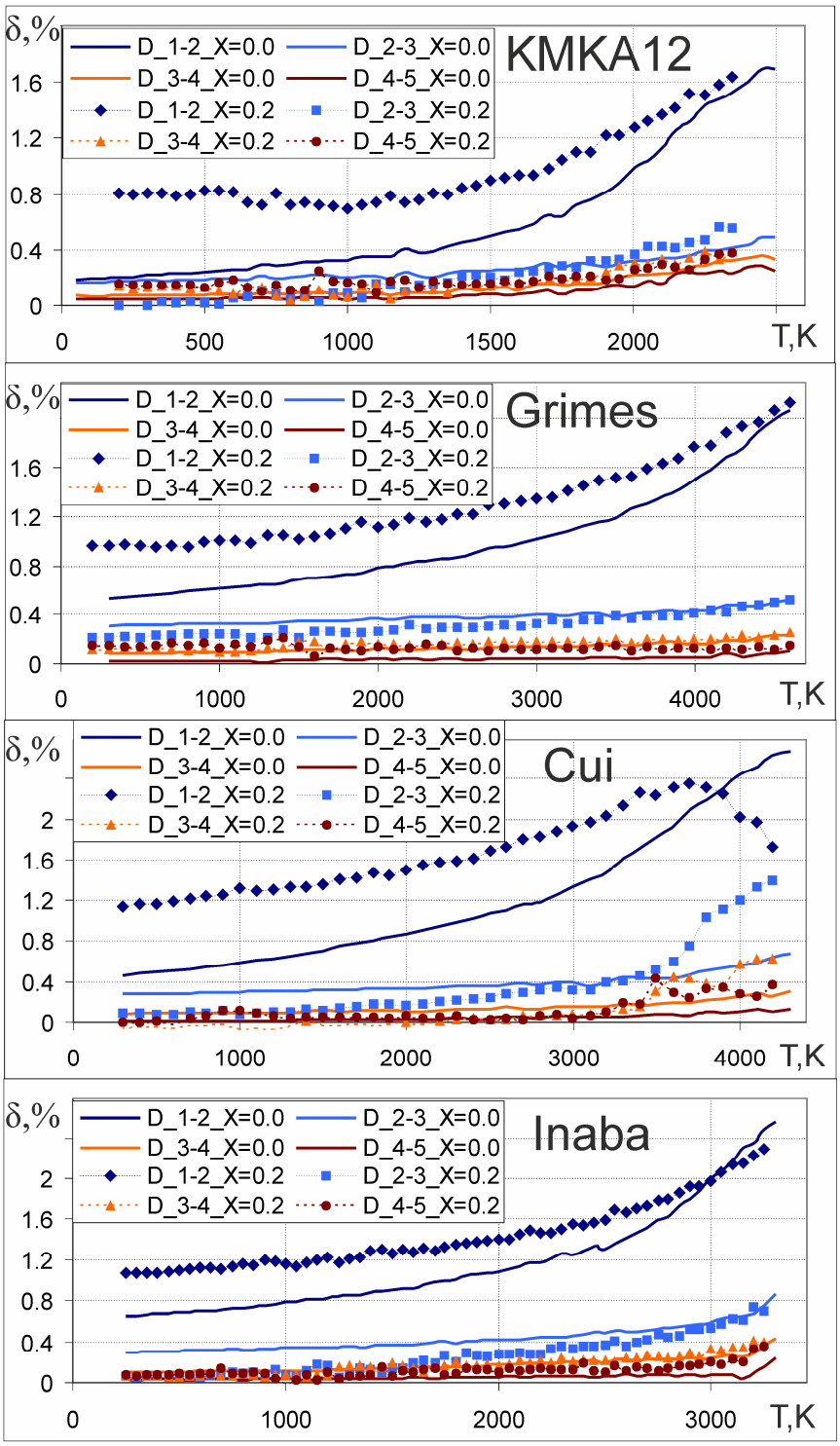

Рис. 8. Temperature dependences of deviations of normal surface interatomic distances (distances between adjacent cationic planes) from the volume IAD of nanocrystal for systems with different interaction potentials.

It follows from the data in Fig. 8 that normal IAD deviations increase with increasing temperature, and this is most pronounced for the D_1-2 IAD between the first and second surface cation layer. Comparison of pure CeO_2 and Gd doped nanocrystals shows that in the doped nanocrystal the distance D_1-2 exceeds the

same distance for pure, and the second and the third near-surface plane on the contrary more contracted than for pure system. The presence of Gd dopant leads to maximum expansion of the outmost cation layer, but cations in next to surface layers remain almost in ideal lattice knots, or, in other words, doped ions localize lattice distortion in the normal direction in the outmost surface layer. With increasing temperature IAD deviations of pure and doped crystals become closer to each other (except for the Cui potential for unknown reasons). We can conclude that in all cases the nanocrystal is expanded along the normal to the (111) surface, and this expansion decreases monotonically towards the nanocrystal center.

Experimental data for IAD in surface layers are not presented in literature, seemingly due to small deviations of these distances from the bulk value. However, surface structures of different types were intensively investigated by quantum-chemical calculation (QCC) along with classical lattice statics and molecular dynamics methods. For example in [19] authors compared simulation results derived by QCC and MD for CeO_2 system, and concluded that results are almost identical. For the (111) surface MD gave expansion of cationic layers of 0.02Å (0.7%), and QCC showed contraction of a similar value. At that, while both GGA and LGA methods in QCC showed contraction, values of contraction differ almost in two times. In the paper [20] it was also noted that the cation sublattice on the (111) surface remains rather intact. Results of QCC with doped systems were not found in literature.

For a more detailed study of tangent expansion-contraction of cationic near-surface (111) facets we selected inner circle region inside each of these facets. A comparison of distances between nearest cations averaged by all cations belong to facet and only inside its inner region gives an estimation of an influence of octahedron truncated corner on cation distortion in (111) facet. Temperature dependences of tangent IAD deviations for pure and doped nanocrystals with different potentials are shown in Fig. 9.

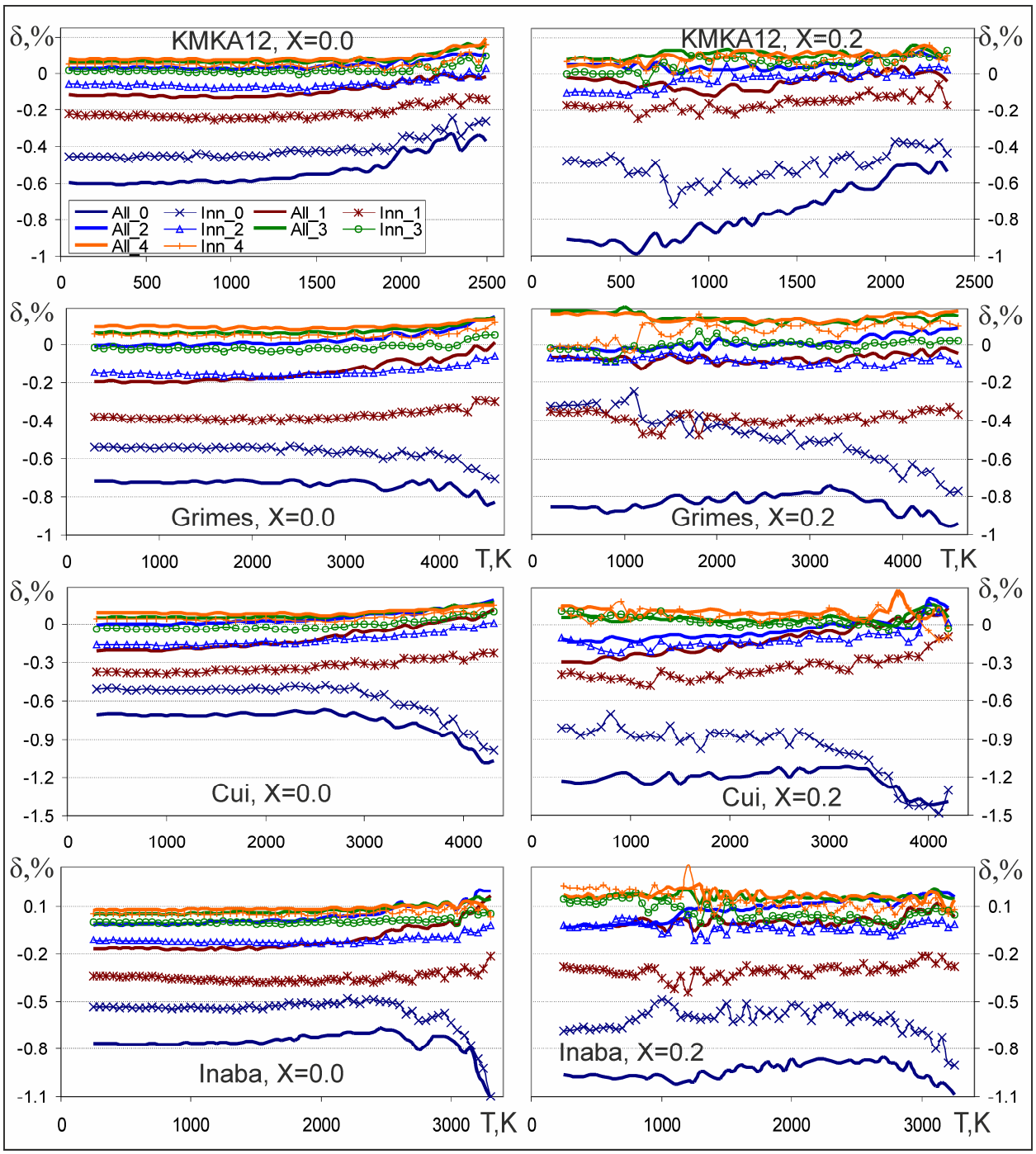

Fig. 9. Temperature dependences of deviations of distances between cations belong to cationic planes parallel to the (111) surface from the corresponding volume distance. Solid lines show distance deviations averaged by all cations belong to facets with a given depth and are marked as "All_"; lines with symbols correspond to distances derived only by cations inside the inner region of the facet and are marked as "Inn_". On the left side results of pure CeO_2 nanocrystal simulation are presented, and on the right side – for doped $Ce_{0.8}Gd_{0.2}O_{1.9}$ system.

It follows from the data in Fig. 9 that for all nanocrystals the outmost cation layer has the largest contraction in the tangent direction, and the contraction inside this plane is larger closer to octahedron truncated corners. Inside the second and

subsequent near-surface layers dependences are reversed – cations are more contracted in the center of a given near-surface (111) facet. In general, contraction decreases with depth toward the nanocrystal center, and corresponding values of the tangent contraction are larger for doped systems than for pure.

Generally during the simulation of 2D-periodic infinite system with the (111) surface the tangent contraction should have zero value. For the finite nanocrystal in vacuum the tangent contraction in surface planes apparently is caused by the surface tension, but we obtained no difference between the values of All_0 (all surface plane cations) and Inn_0 (cations in the inner region) when compared corresponding deviations for systems of 12,000 and 40,500 ions with KMKA12 potentials.

For octahedron truncated corners with the (100) surface type we defined two surface layers and calculated normal IAD between them and tangent IAD between cations in the outmost surface layer. Temperature dependences of IAD deviations are shown in Fig. 10.

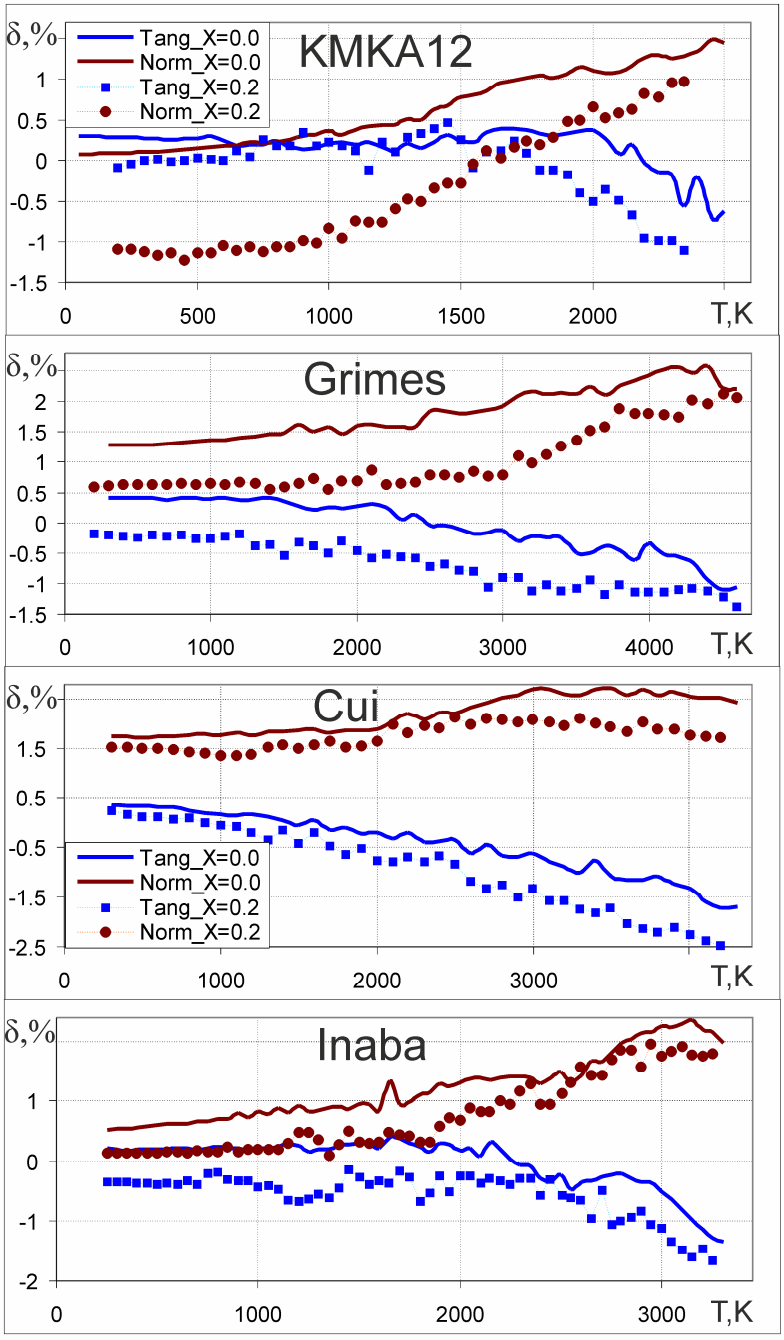

Fig. 10. Temperature dependences of deviations of normal and tangent interatomic distances on octahedron truncated corners with the (100) surface type from the bulk value. Solid lines relate to deviations in the pure CeO_2 system, and symbols – to the doped $Ce_{0.8}Gd_{0.2}O_{1.9}$ nanocrystal.

It follows from the data in Fig. 10 that with increasing temperature normal IAD deviations increase and tangent IAD deviations decrease in all cases. Corresponding IAD deviations are larger in pure than in doped systems.

According to [20] in CeO_2 system with a half of oxygen ions in the outermost layer on the (100) surface (same as in our simulations) interlayer distances in Ce sublattice expanded by 0.05Å (1.8% of the normal IAD deviation

in our terms) compared with the bulk. In the article of Skorodumova et al. [19] expansion or contraction values between cationic surface layers depend on the number and location of outmost oxygen ions. In our MD simulations with all potentials outmost cations are expanded, although the KMKA12 potential show the least expansion value.

3.4. Surface diffusion of cations

Cations in the perfect fluorite crystal lattice are almost motionless compared to anions up to the melting point. However the mobility of cations on the surface is much higher than in the bulk. Calculations of the mean square path (MSP) passed by surface cations (Ce and Gd) along the surface and into the volume of the nanocrystal, according to the method described in section 2.5, are shown in Fig. 11.

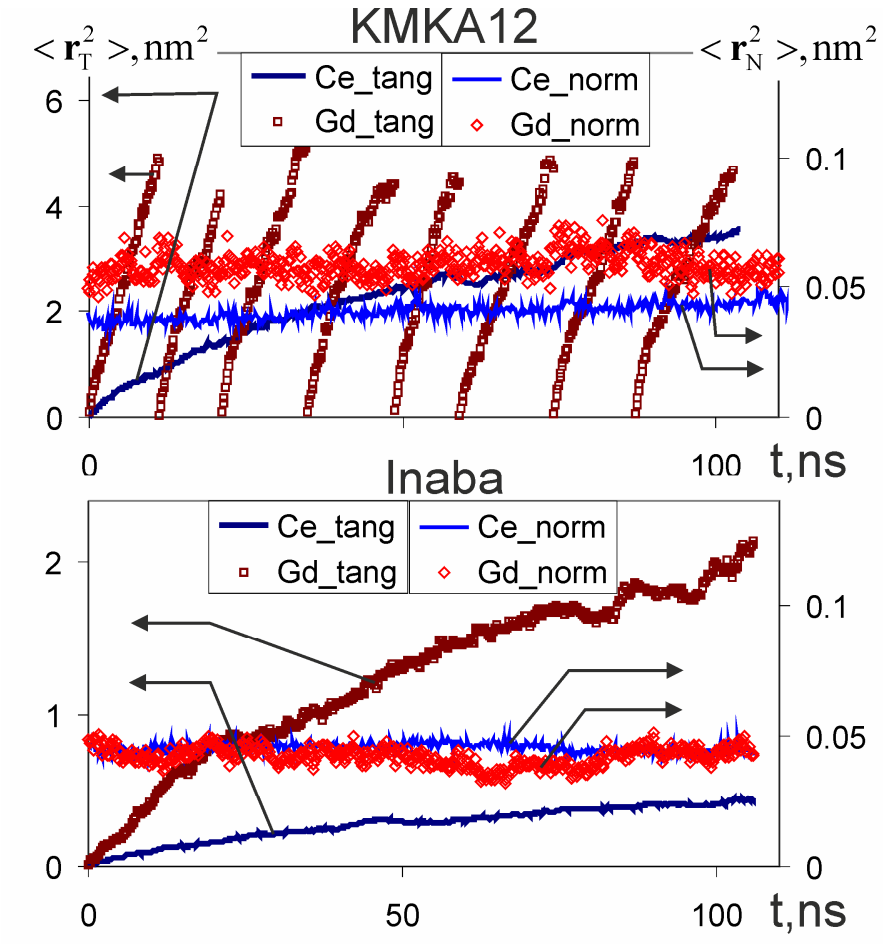

Fig. 11. Tangent (along the surface) and normal (inside the bulk) mean square path of Ce and Gd cations, with KMKA12 (top) and Inaba (bottom) potentials. Tangent MSP relate to the left axis, normal MSP – to the right axis. Nanocrystals consisted of 5939 ions (dopant concentration X=0.2) and both simulation temperatures were approximately equal to 0.8 melting temperature.

From the data in Fig. 11 it is clear that normal MSP of cations for both PPS are almost horizontal, which means that none of cations diffuse into the volume of nanocrystal. All cations move along the surface of the sample, and the displacement along surface coefficient (DaSC) for cations for the simulation time and temperatures explored tends to infinity. However it should be noted that in the liquid state surface cations easy diffuse into the volume. The value of DaSC which is the ratio of tangent MSP to normal MSP angles of slope equals to about 6–7 for cations, as well as for anions.

For a given PPS dopant cations with less charge move faster than host cations. Below surface diffusion coefficients of cations from the data in Fig. 11 derived by (1) with the factor C=4, corresponds to the two-dimensional diffusion, are listed:

Inaba (T=2500 K): $D(Ce) = 7 \cdot 10^{-9} cm^2/s$, $D(Gd) = 2.7 \cdot 10^{-8} cm^2/s$;

KMKA12 (T=2000 K): $D(Ce) = 4.5 \cdot 10^{-8} cm^2/s$, $D(Gd) = 7 \cdot 10^{-7} cm^2/s$.

3.5. Surface diffusion of anions

In fluorite systems the mobility of anions is much higher than of cations, and it is possible to build temperature dependences for anion DaSC, which are shown in Fig. 12 for pure CeO_2. Simulations were carried out down from melting temperature as long as computational power allowed to obtain required statistics for MSD calculations.

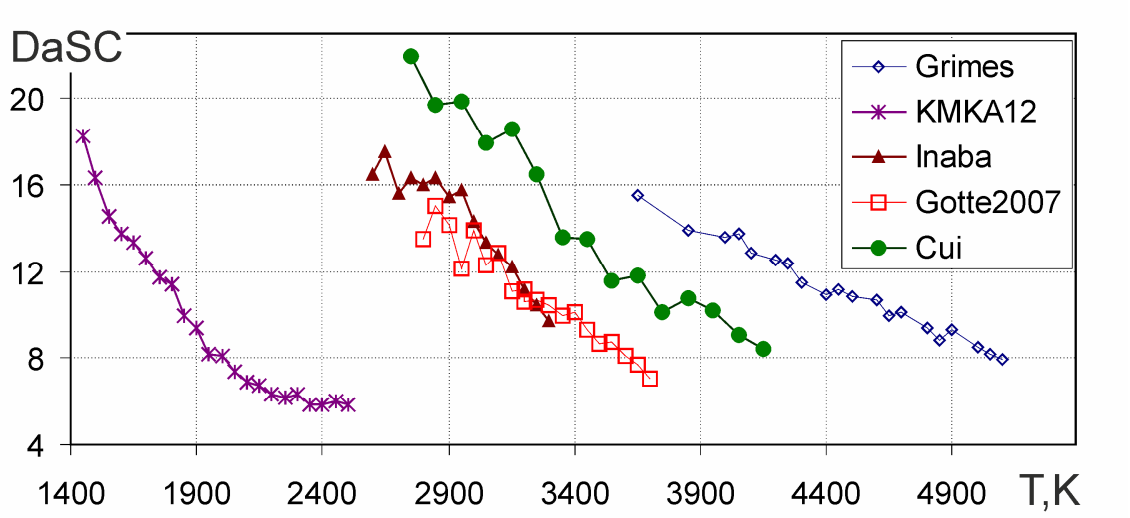

Fig. 12. Temperature dependences of displacement along surface coefficients of anions in pure CeO_2 nanocrystals with different interaction potentials.

For all PPS simulations were performed with crystals of 12000 ions. It follows from the data in Fig. 12 that with all potentials DaSC increases almost linearly with decreasing temperature, and seemingly it means that this property is typical for fluorite systems, than for a given PPS. The DaSC increase means that anion movement becomes more advantageous along the surface than into the volume of nanocrystal with decreasing temperature.

Experimental melting temperature of CeO_2 system is 2873 K and from the data in Fig. 12 an overestimation of the melting point for different PPS can be see. Only KMKA12 potential demonstrate superionic transition for the nanocrystal, and the almost horizontal right part of the DaSC curve corresponds to this phase state.

Gotte2007 PPS in the rigid ion approximation at high temperatures gives instability with the integration step of 0.2 fs (for other PPS this step during simulations was equal to 3.5 fs), the nanocrystal at that was in the crystalline state. The instability consisted in the fact that surface anions at high temperatures may acquire enough kinetic energy to "stick together". We used no cut-off for Gotte2007 potential at small distances. According to the work [13] where the integration step of 0.5 fs was used during simulations of 3D-periodic systems, the “instability” with periodic boundary conditions not occurs. Apparently Gotte2007 PPS is not suitable for the simulation of finite crystals in vacuum at high temperatures.

Temperature dependences of anions DaSC for pure CeO_2 and doped with Gd $Ce_{0.8}Gd_{0.2}O_{1.9}$ nanocrystals with three PPS are shown in Fig. 13.

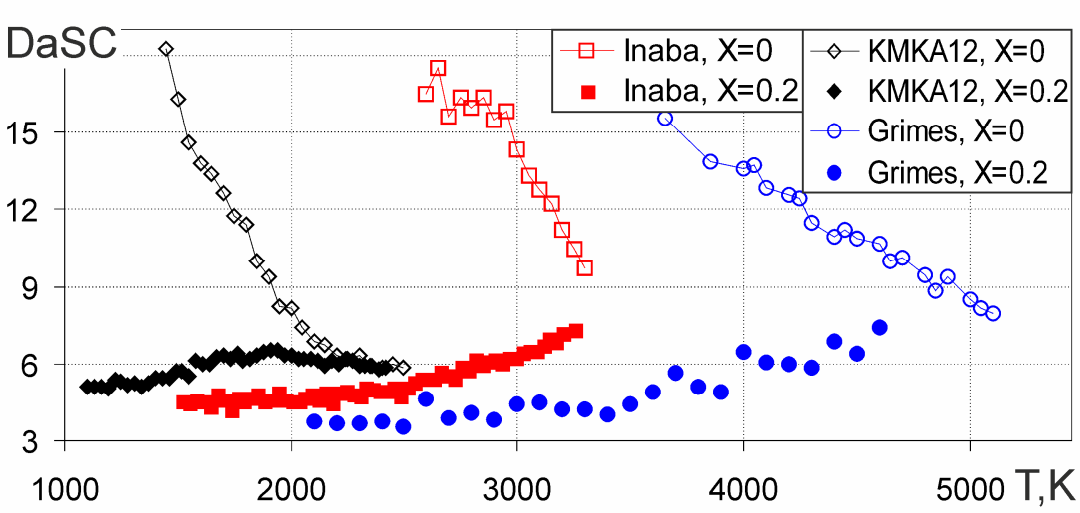

Fig. 13. Comparison of temperature dependences of displacement along surface coefficients for pure and doped nanocrystals of about 12000 ions for three potentials. DaSC for pure CeO_2 are shown by empty symbols and DaSC for $Ce_{0.8}Gd_{0.2}O_{1.9}$ – by solid symbols.

Fig. 13 shows that for the given PPS DaSC for pure and doped nanocrystals converge near the melting temperature. For all PPS the behavior of DaSC is the same - with decreasing temperature DaSC for pure systems sharply increase, and for doped systems DaSC weakly decrease. The lowest values of DaSC were derived for doped systems at low temperatures and were in the range of 4–5 for all PPS, which means that the diffusion of surface anions has mainly the two-dimensional character.

Temperature dependences of DaSC for various dopant concentrations X in the $Ce_{1-X}Gd_XO_{2-X/2}$ system with the KMKA12 potential are shown in Fig. 14.

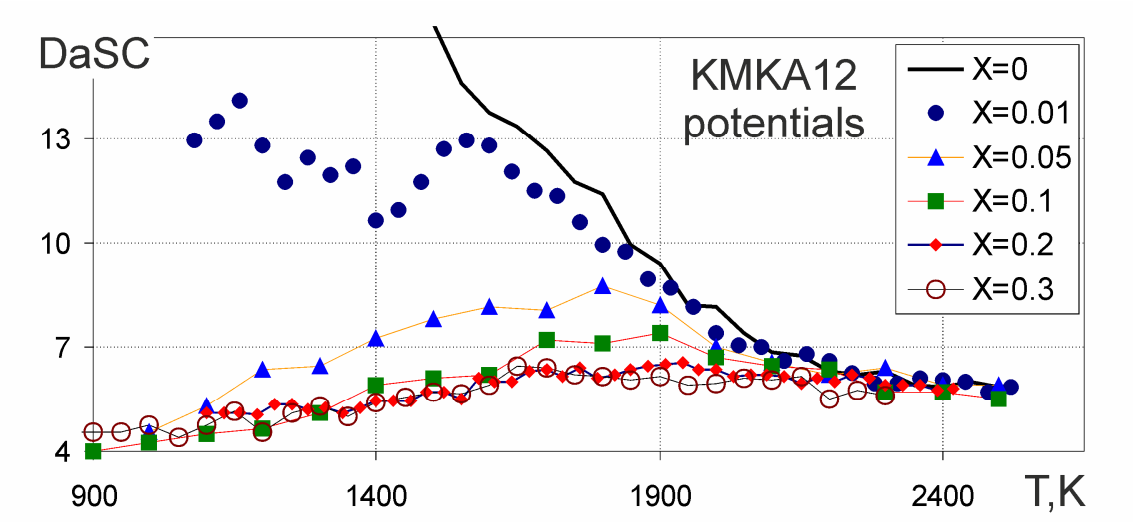

Fig. 14. Comparison of temperature dependences of anion displacement along surface coefficients for nanocrystals with various dopant concentrations X. All simulations were carried out with nanocrystals of about 12000 ions with pair distribution of Gd dopant.

It follows from the data in Fig. 14 that at temperatures close to the melting point DaSC of all systems have the same value. The initial increase of DaSC curves with decreasing temperature from melting point is related to the diffusion by thermal vacancies and a further reduction for doped systems with X≥0.05 is related with the domination of impurity vacancy diffusion. For a system with X=0.01 we give the data below 1400 K, but it should be noted that the finite size of the nanocrystal and the rather small number of impurity vacancies in it leads to a large spread in values and does not give a clear idea of decreasing or increasing DaSC with decreasing temperature.

3.6. Comparison of surface and volume diffusion of anions

Due to the fact that the values of DaSC for surface anions were not less than 4, to derive the diffusion coefficient through MSD in (1) we used a coefficient of C=4 as for the case of two-dimensional diffusion. Calculation of diffusion coefficient (DC) and DaSC values is based on ion positions, but nevertheless they are relatively independent and provide independent information about processes on the surface of nanocrystals.

Volume and surface anion DC for nanocrystals with KMKA12 potential for all investigated impurity concentrations X are shown in Fig. 15.

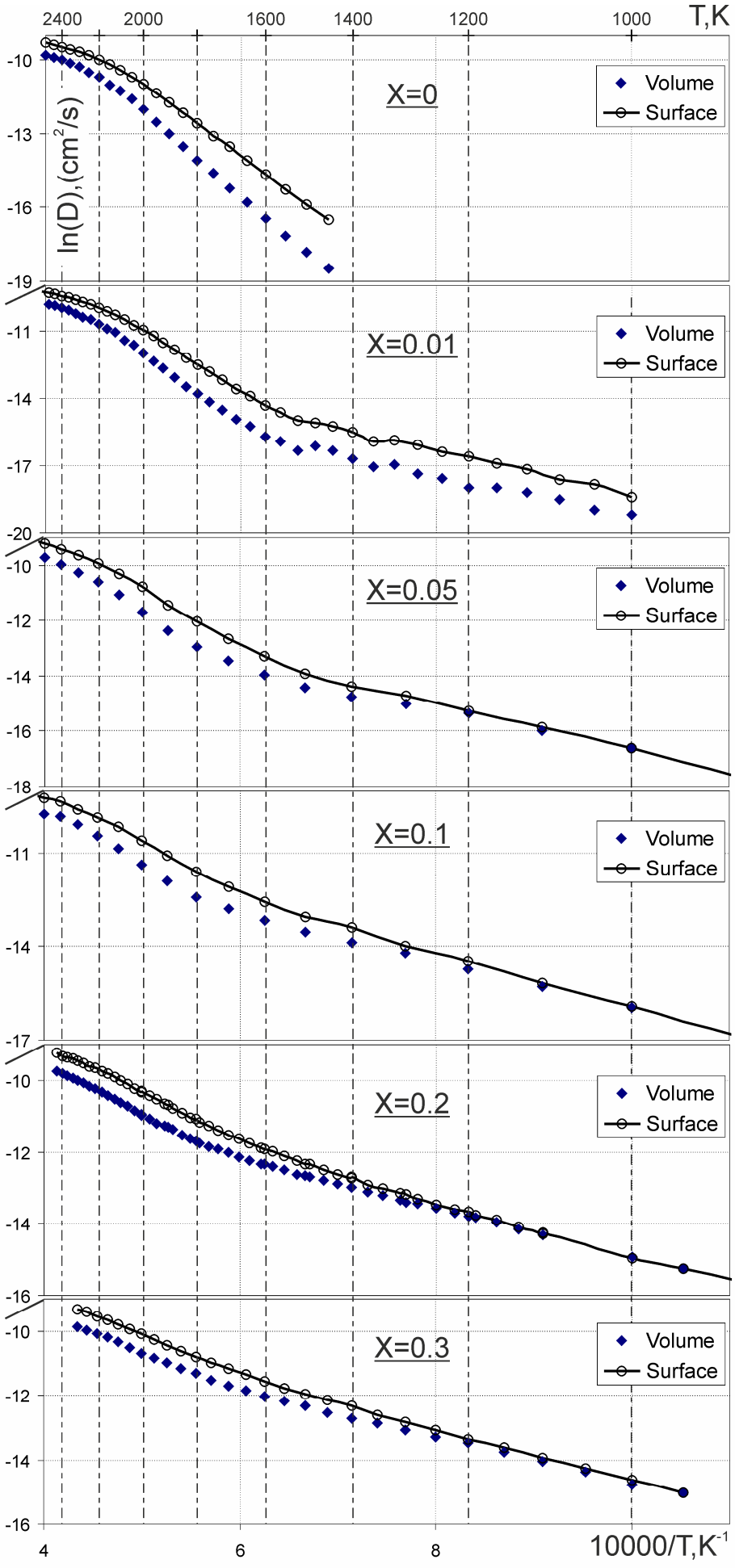
T,K
2400
2000
1600
1400
1200
1000
ln(D),(cm²/s)
X=0
X=0.01
X=0.05
X=0.1
X=0.2
X=0.3
Volume
Surface
10000/T,K⁻¹
4
6
8

Fig. 15. Comparison of temperature dependences of surface and volume anion diffusion coefficients in nanocrystals of about 12,000 ions with KMKA12 potential, for various dopant concentrations X.

High-temperature bend on DC curves corresponds to the superionic transition, and it takes place both in the volume and on the surface of nanocrystal. The next bend at medium temperatures corresponds to the transition from intrinsic to impurity disorder, and again occurs both on surface and in volume. For systems with dopant concentration $X \geq 0.05$ at low temperatures (in the region of the intrinsic disorder) surface DC coincide with volume DC.

From the DC temperature dependence the migration energy E_m and anti-Frenkel (AF) pair formation energy E_{AF} on the surface and in the bulk can be found. To do this, let's consider a system with X=0.01, where the influence of the association of "impurity ion–vacancy" complexes on the diffusion process is minimal compared to systems with a higher Gd dopant concentration, as was shown in [21]. For high temperatures (in the region of intrinsic disorder) diffusion activation energy is the sum of the migration energy and the half of the AF pair formation energy $E_A = E_m + 0.5 \cdot E_{AF}$. At temperatures T<1500 K the diffusion by impurity vacancies dominates, so we assume that the anion diffusion activation energy equals to the migration energy, neglecting the contribution of the association energy of vacancy with an impurity cation. From the data showed in Fig. 15 we obtained migration energies E_m(surf)=0.82eV, E_m(vol)=0.77eV, and AF pair formation energies E_{AF}(surf)=3.01eV, E_{AF}(vol)=4.04eV on the surface and in the volume respectively. For the pure CeO_2 nanocrystal, taking the above values of migration energies, we got AF pair formation energies equal to E_{AF}(surf)=3.43eV и E_{AF}(vol)=4.32eV. It follows from these figures that migration energies for anions approximately equal on the surface and in the volume of the nanocrystal, but AF pairs are formed on a surface by about 1eV easier than in the bulk.

The equality of migration energies on the surface and in the bulk of nanocrystal in impurity disorder region (medium and low temperatures) can be explained by the structure of the nanocrystal surface. Diffusion occurs via vacancy

mechanism, so anion hops to the neighbor impurity vacancy. Surface of (111) type is dominate, and surface anion is surrounded by three cations on the distance of about $a\sqrt{3}/4$ (where a is the lattice parameter), same as in the bulk, and by six anions belong to the plane of this surface. The distance between nearest anions **on** the surface is about $a\sqrt{2}/2$ and considerably higher than distance between nearest anion in the bulk $a/2$. Thus, surface anion should move the longer distance during the diffusion hop, than bulk anion, or, in other words, surface anion should make double hop compared with bulk anion.

For pure CeO_2 surface DC of anions exceeds volume DC for all temperatures studied, and the lower the temperature, the greater the difference. Deviations of surface DC from volume DC versus the simulation temperature for various dopant concentrations X are shown in Fig. 16.

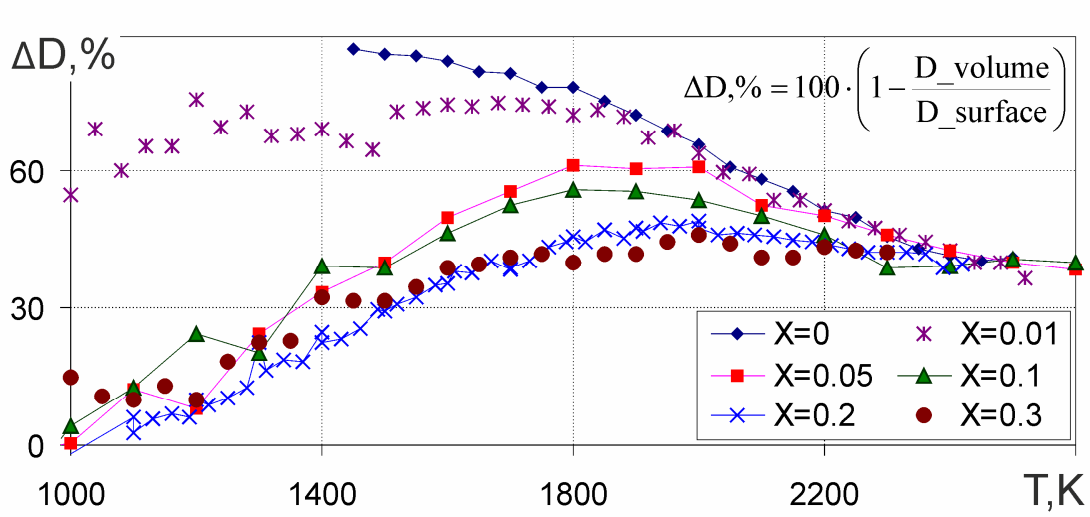

Fig. 16. Temperature dependences of deviations between surface and volume anion diffusion coefficients for various dopant concentrations X. Nanocrystals of about 12000 ions were simulated with KMKA12 potential.

It follows from the data in Fig. 16 near the melting point deviations of anion DC equal to about 40% for all dopant concentrations X. At low temperatures the surface anion DC is twice the volume DC for the pure CeO_2 nanocrystal, while in systems with impurity concentration $X \geq 0.05$ surface and volume DC are approximately equal.

Such behavior may be explained from the standpoint of the competition of diffusion mechanisms corresponding to intrinsic (thermal) and impurity disorder. The formation energy of thermal vacancies on the surface is smaller than inside the volume at the same migration energies. Therefore with decreasing temperature more thermal vacancies are formed on the surface, which leads to increasing of surface DC in comparison with volume DC, in the temperature region where the impurity disorder is not predominate. However, at low temperatures the number of thermal vacancies becomes small compared with impurity vacancies on the surface and in the volume of the nanocrystal, causing the equality of volume and surface DC. In the case of X=0.01 at temperatures of T=1000 K the average number of thermal vacancies on the surface seems to be comparable with the number of impurity vacancies, which leads to the deviation of about 60%.

All surface anion diffusion coefficients for a visual comparison are shown in Fig. 17.

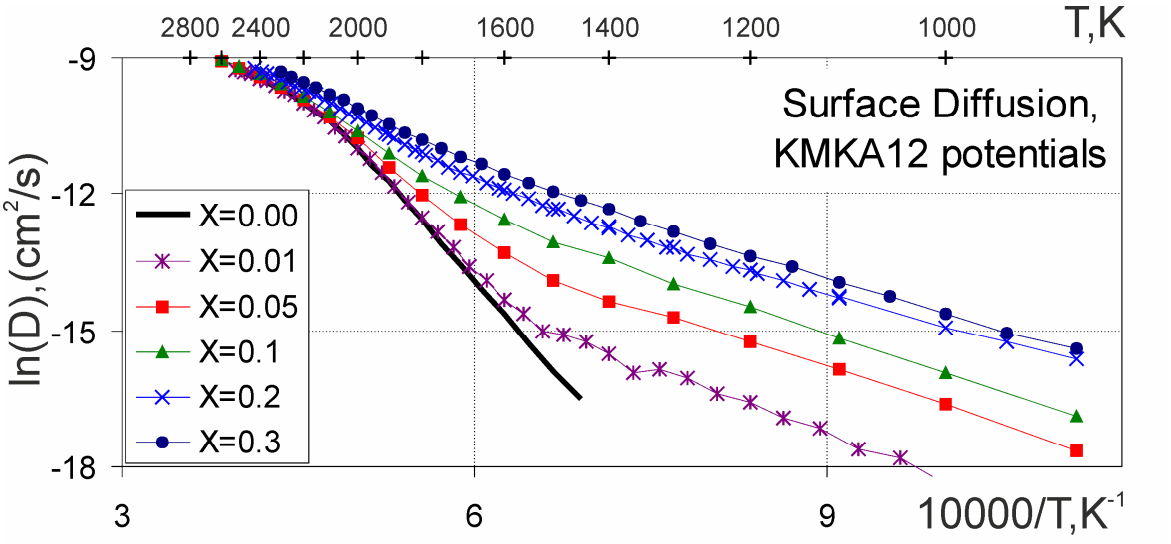

Fig. 17. Temperature dependences of surface diffusion coefficients of anions for nanocrystals of about 12000 ions with various dopant concentration X, simulated with KMKA12 potential.

For all temperatures surface DC are large for systems with higher dopant concentration, at that its absolute values converge near the melting point.

Bends on curves of surface DC, corresponding to the superionic transition and to the transition from intrinsic to impurity disorder, are clearly observed, as in the case of volume DC.

4. Conclusions

1. Methods of dynamic detection of the surface of $Ce_{1-X}Gd_XO_{2-X/2}$ nanocrystals and decomposition of surface ion displacement on the tangent (along the surface) and normal (into the volume) components were developed. With the four pair potential sets near-surface interatomic distances of cations and diffusion coefficients of surface anions were investigated over a wide range from room temperature to the melting point.
2. The relaxation process of the original cubic nanocrystal in its equilibrium shape of a truncated octahedron was studied in detail. For nanocrystals of various sizes surface areas of (100) and (111) types were calculated, and a maximum of the area ratios S(100)/S(111) was found for nanocrystals of 6000–12000 ions (8–10 nm).
3. For all investigated pair potentials the character of temperature dependences of near-surface interatomic distances between cations is the same. Surface layers in the nanocrystal are expanded perpendicular to the (111) surface, but inside a given layer cations are contracted along the surface, which seemingly is due to the surface tension.
4. Diffusion of surface cations has a two-dimensional character. At the temperature equals to 0.8 melting temperature during simulation time of about 100 ns cations moved only along the nanocrystal surface, but not into the bulk.
5. Temperature dependences of diffusion coefficients of surface anions were investigated, and they have the same behavior for a given dopant concentration with all pair potentials studied. Although anions moved into the bulk, unlike cations, generally anions moved along the nanocrystal surface.
6. For nanocrystals with various dopant concentrations with KMKA12 potential temperature dependences of anion diffusion coefficients in the volume and on the surface were compared. For the surface the superionic transition is observed, similar as in the bulk.

7. Anion migration energies on the surface and in the bulk are the same and equal to 0.82eV and 0.77eV respectively, at that the formation energy of thermal anti-Frenkel pair on the surface is 3eV and 1eV less than the formation energy of this pair in the nanocrystal volume.

8. For all systems with impurity concentration $X \geq 0.05$ at low temperatures $T<1200$ K anion diffusion coefficients on the surface and in the bulk coincide with each other.

References

[1] H. Nörenberg, G. A. D. Briggs. Physical Review Letters 79, 21 (1997) 4222-4225.

[2] D.R. Mullins, P.V. Radulovic, S.H. Overbury. Surface Science 429 (1999) 186-198.

[3] A. Pfau, K.D. Schierbaum. Surface Science 321 (1994) 71-80.

[4] Claude Binet, Ahmed Badri, Jean-Claude Lavalley. J. Phys. Chem. 98 (1994) 6392-6398.

[5] P.S. Manning, J.D. Sirman, J.A. Kilner. Solid State Ionics 93 (1997) 125-132.

[6] M. Veronica Ganduglia-Pirovano, Alexander Hofmann, Joachim Sauer. Surface Science Reports 62 (2007) 219-270.

[7] S.I. Potashnikov, A.S. Boyarchenkov, K.A. Nekrasov, A.Ya. Kupryazhkin. J. Nucl. Mater. 419 (2011) 217-225.

[8] M.A. Kovalenko, A.Ya. Kupryazhkin. J. Nucl. Mater. 430 (2012) 12-19.

[9] Hideaki Inaba, Rie Sagawa, Hideko Hayashi, Katsuyuki Kawamura. Solid State Ionics 122 (1999) 95-103.

[10] A. Gotte, D. Spångberg, K. Hermansson, M. Baudin. Solid State Ionics 178 (2007) 1421– 1427.

[11] Licia Minervini, Matthew O. Zacate, Robin W. Grimes. Solid State Ionics 116 (1999) 339–349.

[12] Zhiwei Cui, Yi Sun, Yunjun Chen, Jianmin Qu. Solid State Ionics 187 (2011) 8–18.

[13] Dilpuneet S. Aidhy, Dieter Wolf, Anter El-Azab. Scripta Materialia 65 (2011) 867–870.

[14] G. S. Herman. Physical Review B 59, 23 (1999) 14899-14902.

[15] Thi X. T. Sayle, Stephen C. Parker, Dean C. Sayle. Faraday Discussions 134 (2007) 377–397.

[16] R.W. Hockney, J.W. Eastwood. Computer simulation using particles, McGraw-Hill Inc (1981).

[17] A. S. Barnard, A. I. Kirkland. Chem. Mater. 20 (2008) 5460–5463.

[18] Martin R. Castell. Physical Review B 68 (2003) 235411.

[19] N. V. Skorodumova, M. Baudin, K. Hermansson. Physical Review B 69 (2004) 075401.

[20] Zongxian Yang, Tom K. Woo, Micael Baudin, Kersti Hermansson. J. Chem. Phys 120, 16 (2004) 7741-7749.

[21] M.A. Kovalenko, A.Ya. Kupryazhkin. J. Nucl. Mater. 440 (2013) 158–168.